Climate of the Past

Open Access

Discussions

A GCM comparison of Plio–Pleistocene interglacial–glacial periods in relation to Lake El'gygytgyn, NE Arctic Russia

A. J. Coletti[1], R. M. DeConto[1], J. Brigham-Grette[1], and M. Melles[2]

[1]Department of Geosciences, University of Massachusetts, Amherst, MA 01003, USA
[2]Institute of Geology and Mineralogy, University of Cologne, Zuelpicher Strasse 49a, 50674 Cologne, Germany

Correspondence to: A. J. Coletti (ajcolett@geo.umass.edu) and R. M. DeConto
(deconto@geo.umass.edu)

Discussion Paper | Discussion Paper | Discussion Paper | Discussion Paper

CPD

10, 3127–3161, 2014

A GCM comparison of Plio–Pleistocene interglacial–glacial periods

A. J. Coletti et al.

Title Page

Abstract	Introduction
Conclusions	References
Tables	Figures

◄◄ | ►►

◄ | ►

Back | Close

Full Screen / Esc

Printer-friendly Version

Interactive Discussion

A GCM comparison of Plio–Pleistocene interglacial–glacial periods

A. J. Coletti et al.

Abstract

Until now, the lack of time-continuous, terrestrial paleoenvironmental data from the Pleistocene Arctic has made model simulations of past interglacials difficult to assess. Here, we compare climate simulations of four warm interglacials at Marine Isotope Stage (MIS) 1 (9 ka), 5e (127 ka), 11c (409 ka), and 31 (1072 ka) with new proxy climate data recovered from Lake El'gygytgyn, NE Russia. Climate reconstructions of the Mean Temperature of the Warmest Month (MTWM) indicate conditions 2.1, 0.5 and 3.1 °C warmer than today during MIS 5e, 11c, and 31 respectively. While the climate model captures much of the observed warming during each interglacial, largely in response to boreal summer orbital forcing, the extraordinary warmth of MIS 11c relative to the other interglacials in the proxy records remain difficult to explain. To deconvolve the contribution of multiple influences on interglacial warming at Lake El'gygytgyn, we isolated the influence of vegetation, sea ice, and circum-Arctic land ice feedbacks on the climate of the Beringian interior. Simulations accounting for climate-vegetation-land surface feedbacks during all four interglacials show expanding boreal forest cover with increasing summer insolation intensity. A deglaciated Greenland is shown to have a minimal effect on Northeast Asian temperature during the warmth of stage 11c and 31 (Melles et al., 2012). A prescribed enhancement of oceanic heat transport into the Arctic ocean has some effect on Beringian climate, suggesting intrahemispheric coupling seen in comparisons between Lake El'gygytgyn and Antarctic sediment records might be related to linkages between Antarctic ice volume and ocean circulation. The exceptional warmth of MIS 11c remains enigmatic however, relative to the modest orbital and greenhouse gas forcing during that interglacial. Large Northern Hemisphere ice sheets during Plio-Pleistocene glaciation causes a substantial decrease in Mean Temperature of the Coldest Month (MTCM) and Mean Annual Precipitation (PANN) causing significant Arctic aridification. Aridification and cooling can be linked to a combination of mechanical forcing from the Laurentide and Fennoscandian ice sheets on

mid-tropospheric westerly flow and expanded sea ice cover causing albedo-enhanced feedback.

1 Introduction

Knowledge of Pleistocene climate history has increased dramatically over the past three decades, however existing records remain strongly biased toward an oceanic viewpoint, due to the lack of long terrestrial archives. In the context of future warming, it is clearly important to understand the effects of warming on the terrestrial Arctic, the strength of polar amplification, and systemic teleconnections to and from other latitudes. Past warm periods known as Interglacials over the past 2.8 million years provide a means of studying climates warmer than today, giving us some indication of possible outcomes of current trends.

In 2009, a multinational team of scientists drilled a sediment core from a 25 km wide impact crater lake named "Lake El'gygytgyn" (alternatively, Lake "E"), in northeast Siberia. The core contained the longest Arctic terrestrial record ever recovered, extending back ∼ 3.5 million years. The sediment core revealed evidence for periods of exceptional warmth during Pleistocene interglacials, as defined by marine benthic δ^{18}O records (Lisiecki and Raymo, 2005). It has been shown that Marine Isotope Stage(s) 5e, 11c and 31 were among the warmest interglacials in the Pleistocene Arctic (Melles et al., 2012).

To explore the sensitivity of northwestern Beringia to interglacial forcing and the mechanisms responsible for the observed climate changes, we use a Global Climate Model coupled to an interactive vegetation model to simulate the terrestrial Arctic's response to the greenhouse gas and astronomical forcing associated with each specific interglacial (Yin and Berger, 2011). A range of glacial land surface, Arctic Ocean, and sea ice boundary conditions are imposed to test the response of the region to changes in circum-Arctic ice sheets and possible changes of ocean heat transport into the Arctic Ocean. The results are then compared to the Lake El'gygytgyn multiproxy analysis

and assessed relative to teleconnections implied by other far field records, including Antarctica.

2   Model and experimental design

All global climate simulations discussed herein were performed using the current (2010) version of the Global ENvironmental and Ecological Simulation of Interactive Systems (GENESIS) Global Climate Model (GCM) version 3.0 (Thompson and Pollard, 1997). GENESIS is an atmosphere, land-surface, ocean, snow, sea ice, ice sheet and vegetation coupled model. As used here, spectral resolution of the atmosphere GCM is T31 resolution (3.75° lat. × 3.75° long.) with 18 vertical levels (Thompson and Pollard, 1997). The AGCM is coupled to 2° × 2° soil, snow, vegetation, ocean, and sea ice model components. The GCM is interactively coupled to the BIOME4 (Kaplan, 2003) vegetation model, a coupled carbon and water flux model that predicts equilibrium vegetation distribution, structure and biogeochemistry using monthly mean climatologies of precipitation, temperature and clouds simulated by the GCM. Vegetation distributions take the form of 27 plant biomes including 12 plant functional types (PFTs) that represent broad, physiologically distinct classes ranging from cusion-forbs to tropical rain forest trees (Kaplan, 2003). GENESIS includes options for coupling to an Ocean General Circulation Model (Alder et al., 2011) or a non-dynamical, slab ocean model that incorporates heat transfer, calculations of sea-surface temperatures (SST) and feedbacks operating between ocean surface and sea ice. The slab mixed layer ocean model is used here to allow multiple simulations to be performed with and without imposed perturbations of surface ocean conditions. This version of the GCM has a sensitivity to $2 \times CO_2$ of 2.9 °C, without GHG, vegetation or ice sheet feedbacks. Greenhouse gasses and orbital parameters for each interglacial were prescribed according to ice core records (Loulergue et al., 2008; Lüthi et al., 2008; Schilt et al., 2010) and standard astronomical solutions (Berger, 1978).

The strategy adopted here was to target Marine Isotope Stage (MIS) 1 (11 ka), 5e (127 ka), 11c (409 ka) and 31 (1072 ka), corresponding to the timing of peak summer warmth observed at the Lake and identified as "super-interglacials" by Melles et al. (2012). Equilibrium simulations were performed at the time of peak boreal summer insolation assuming the real climate system equilibrated within a half-precession cycle. Temperature and precipitation data were 10 year averages taken from the 30 to 40 year equilibrated simulation. Preliminary analysis of pollen assemblages in the Lake El'gygytgyn core are assumed to provide a record of peak summer temperatures allowing our focus to be on data-model comparisons of warmest monthly mean climate (July). Simulations of present day (355 ppm$_v$ pCO$_2$) and pre-industrial climate (280 ppm$_v$ pCO$_2$) were run as control experiments to determine the fidelity of the model's representation of Holocene climate in Beringia and to provide a baseline for comparing super-interglacial simulations. In order to understand the effects a cold, Pliocene orbit, additional sensitivity tests of Lake El'gygytgyn to changing boundary conditions associated with the buildup of major Northern Hemisphere ice sheets was also simulated mimicking glacial-like conditions within the region.

2.1 MIS 1, 9 ka

MIS-1 represents the last 11 000 years and its onset roughly coincides with the end of the Younger-Dryas. Peak boreal summer insolation occurs ∼ 9 ka, when summer insolation was ∼ 510 W m^{-2} at 65° N, relative to 446 Wm^{-2} today. Proxy indicators suggest conditions were warmer than present (+1.6 °C over western Arctic and +2 to 4 °C in circum-Arctic) with lush birch and alder shrubs (Melles et al., 2012) dominating vegetation around the lake. This period, known as the Holocene Climate Optimum (HCO), was spatially variable, with the biggest affect on the high latitudes, with minimal warming in the mid-latitudes and tropics (Kitoh and Murakami, 2002).

2.2 MIS-5e, 127 ka

Interglacial-5e, also known as the Last InterGlacial (LIG), is one of the warmest in-terglacials of the Pleistocene and lasted roughly ∼ 12–10 ka (130 to 116 ka). High obliquity, eccentricity and the timing of perihelion (precession) combined to produce high intensity boreal summer insolation at around 127 ka. Greenland ice core records (Dahl-Jensen et al., 2013) suggest warm conditions throughout the Arctic with sum-mer warming up to +8 °C over northeast Greenland, but paradoxically, only a modest reduction in the size of the Greenland Ice Sheet (GIS). Studies involving Sr – Nd – Pb isotope ratios of silt-sized sediment discharged from southern Greenland suggest that no single southern Greenland geologic terrain was completely deglaciated during the LIG, however, some southern GIS retreat was evident (Colville et al., 2011). A pre-vious model study of MIS-5e by (Yin and Berger, 2011) involved running a model of intermediate complexity to test relative contributions of Greenhouse Gas (GHG) and insolation forcing on LIG warmth. They found that GHGs play a dominant role on the variations of the annual mean temperature of both the globe and the southern high latitudes, whereas, insolation plays a dominate role on the on precipitation and north-ern high latitude temperatures and sea ice (Yin and Berger, 2011). Similarly, enhanced solar anomalies during MIS-5e was shown to have driven significant summer (JJA) Siberian warming supporting warm temperatures throughout the Arctic (Otto-Bliesner et al., 2006).

The simulation of LIG shown here is used to compare with the paleoenvironmental conditions in the Arctic during this period of and investigate temperature, vegetation and precipitation and correlate the data to pollen proxy analysis. Orbital and GHG values are estimated for 127 ka; peak warmth during MIS 5e.

2.3 MIS-11c, 409 ka

Interglacial-11c is another exceptionally warm interglacial that lasted from 428 to 383 ka (∼ 45 ka). Sediment records containing information on MIS-11 are generally lacking

(Miller et al., 2010). Unlike the other interglacials, insolation forcing during MIS-11c was remarkably long, with two insolation maxima anomalies at ∼ 409 ka and 423 ka, apparently creating extensive warmth throughout the Arctic (Melles et al., 2012). Unlike MIS-5e, there is evidence that the GIS may have been much reduced in size (Raymo and Mitrovica, 2012; Willerslev et al., 2007), with lush boreal forest covering most of southern Greenland (de Vernal and Hillaire-Marcel, 2008). Particularly warm conditions are also suggested by pollen records analyzed from Lake Biwa (Tarasov et al., 2011) located in Shiga Prefecture, Japan. Likewise, a study from Lake Baikal also indicates warmer than modern temperatures with a "conifer optimum" suggesting not only warmer conditions, but also less continental aridity, perhaps influenced by higher sea levels and reduced continentality (Prokopenko et al., 2010).

Three different simulations (Table 1) were run to test the sensitivity of the lake region to MIS-11c forcing. The first simulation uses default boundary conditions, including a modern Greenland Ice Sheet (MIS11GIS). The second simulation tests the sensitivity of the Arctic to an ice-free Greenland (MIS11NG). In this simulation, the GIS was removed and topography of Greenland was corrected for glacial isostatic adjustment (GIA) within the appropriate model topography files, to test an extreme scenario involving a completely ice-free Greenland. The final sensitivity experiment includes an increase in sub-sea ice surface heat flux from $2\,W\,m^{-2}$ in our modern control, to $10\,W\,m^{-2}$ (additional $+8\,W\,m^{-2}$) to test the Beringian sensitivity to a mostly ice-free Arctic Ocean. The increased heat flux assumes an extreme ∼ 3 Sverdrup (Sv) increase in Bering Strait throughflow and a 4 °C temperature contrast between North Pacific and North Polar surface water (Melles et al., 2012, supplemental). The additional heat flux convergence was used to mimic the potential influence of a wider and deeper Bering Strait during times of higher sea level. Using the predictive BIOME4 vegetation model, direct comparisons of observed and modeled Arctic vegetation within the Beringian region and at Lake El'gygytgyn can be made. Furthermore, simulations using prescribed distributions of are used to quantify the local effect of changing vegetation cover around the lake region.

2.4 MIS-31, 1072 ka

MIS-31 ($\sim$ 1072 ka) (Lisiecki and Raymo, 2005) has only been identified in a few Arctic records prior to Lake E. The Interglacial represents one of the last 41 ka glacial cycles and is best known for extreme warmth in circum-Antarctica ocean waters induced by a deterioration of the Polar Front (Scherer et al., 2008) and the collapse of the marine based West Antarctic Ice Sheet (WAIS) (DeConto et al., 2012; Pollard and De-Conto, 2009), by intrusion of warm surface waters onto Antarctic continental shelves. On Ellesmere Island, Fosheim Dome includes terrestrial deposits that date to $\sim$ 1.1 Ma, which contains fossil beetle assemblages dated as MIS 31, suggesting temperatures of 8 to 14 °C above modern values (Elias and Matthews Jr., 2002). It is speculated, like MIS-11c, the Arctic may have been too warm to support a Greenland Ice Sheet therefore, the Greenland Ice Sheet may have been substantially reduced in size, or possibly nonexistent (Melles et al., 2012; Raymo and Mitrovica, 2012). Hence, MIS model runs with and without a GIS were executed to show sensitivity and forcing feedback for these scenarios (Table 1).

2.5 Glacial boundary conditions: $\sim$ 2.7 Ma

An additional sensitivity test of Lake El'gygytgyn to changing boundary conditions associated with the buildup of major Northern Hemisphere ice sheets was also simulated and related to pollen analysis at $\sim$ 2.7 Ma in the lake core. Such a substantial cooling in the Arctic has been demonstrated to coincide with a dramatic decrease in PANN values around the lake (Brigham-Grette et al., 2013). Climate model simulations (Table 2) were run with 300 ppm of $p\text{CO}_2$ and a cold, boreal summer orbit, like that of 116 ka (Brigham-Grette et al., 2013). The simulations represent conditions similar to the late Pliocene, with an orbit favorable for the growth of major Northern Hemisphere ice sheets.

Two simulations (Table 2) were run using the GCM with (3HL116K) and without (3NG116K) Northern Hemisphere ice sheets. In both cases, the GCM was run to equi-

librium with averages calculated from the last 10 years of the model's history files. The first simulation used ice-free Northern Hemispheric climate conditions, while the second simulation adds the Greenland, Laurentide and Fennoscandian ice sheets, based on the LGM ice volume from ICE 4G (Brigham-Grette et al., 2013; Peltier, 1994) including a decreased sea level. This simple sensitivity test is used to show the effect of large Northern Hemisphere ice sheets on Arctic climate.

3 Results

3.1 Control simulations

3.1.1 Modern simulation

In order to test the model's ability to accurately simulate 2 meter (2 m) surface temperature and precipitation at the lake, model outputs in the grid cell containing the lake were directly compared to modern observations and reanalysis products. The model grid cell elevation (536 m) is close to the actual elevation of the lake (492 m) to preclude the need for lapse rate corrections. The control simulation yielded mean annual 2 m air temperature (MAAT) of $-9\,°C$, which is within the range of uncertainty ($-10.3 \pm 1.1\,°C$), recorded by Nolan and Brigham-Grette (2006) in 2002, using weather station measurements around the lake. Simulated summer (JJA) and Mean Temperature of the Warmest Month (MTWM; July) surface temperatures are 10.2 and $12\,°C$, respectively which is on par with the modern climatology of the region based on reanalysis (Kalnay et al., 1996).

To further test the validity of the GCM temperatures, a comparison was made with National Center for Environmental Prediction (NCEP) Reanalysis data. The difference indicates that the GCM is only $+0.5\,°C$ warmer than the modern reanalysis data in the lake region, signifying relatively reliable temperature results. Yet, the GCM produces

a warm bias over Greenland and parts of Northeastern Canada, and a cold bias in central, interior Russia compared to NCEP.

Control simulation of Mean Annual Precipitation (PANN) was rather high, indicating ~475 mm yr^{-1} of liquid precipitation. This is substantially greater than Nolan and Brigham-Grette (2006) analysis of 178 mm yr^{-1} from measurements taken over single-year, however this apparent data-model mismatch may in part be associated with high inter-annual variability within the model simulations and the actual climate. Mean summer precipitation in the lake region is ~63 mm month^{-1} similar to observations noted by Melles et al. (2012); Nolan and Brigham-Grette (2006). Moreover, simulated winter (December, January, and February) precipitation is rather dry, with amounts in excess of ~26 mm month^{-1}. It is important to reiterate that the observed Lake El'gygytgyn climatology is fairly dry and the GCM exhibits an apparent wet bias in regards to annual precipitation, in our study region.

Modern model simulations of biome distribution show the lake region and most of the Beringian interior is covered by Evergreen taiga/montane forest, with some exception along the coasts (East Siberian Sea, Chukchi Sea, Beaufort Sea), where Dwarf and Shrub tundra are dominant. Additionally, deciduous taiga/montane forest heavily dominates interior Siberia and the northern coast with a few areas of shrub tundra and grassland mixed in. Warm and cool mixed forests seem to dominate further South, on Kamchatka Peninsula. Kappa-statistics of model-generated vs. observed Arctic biome distributions show that this model does a good overall job of simulating modern vegetation, even without bias corrections (Kaplan, 2003; Koenig et al., 2012).

3.1.2 Pre-industrial

Simulations of pre-industrial 2 m MAAT and MTWM at Lake El'gygytgyn are −12 and 10.3 °C, respectively. This is to be expected, as pre-industrial GHG levels are lower than today. Furthermore, Earth's orbital configuration, specifically obliquity, has changed little in 120 years. Thus, lake regional annual air and July temperatures are −3 °C and −1.7 °C cooler than those of the modern simulations, respectively. Similarly, summer

A GCM comparison of Plio–Pleistocene interglacial–glacial periods

A. J. Coletti et al.

temperatures (8 °C) are on the order of −2.2 °C cooler. GHG radiative forcing from a combination of CO_2, CH_4, and N_2O atmospheric mixing ratios implies a $1.8\,W\,m^{-2}$ reduction relative to modern GHG radiative forcing which accounts for the most of the difference in modern vs. pre-industrial climatologies. Generally, PANN values in the cooler, pre-industrial simulation showed slightly lower values than that of our modern precipitation values. Annual precipitation was $\sim 438\,mm\,yr^{-1}$ ($+122\,mm\,yr^{-1}$ relative to obs.). Mean winter (DJF) precipitation was $\sim 24\,mm\,month^{-1}$, while mean summer precipitation was $43\,mm\,month^{-1}$, indicating −2 and −20 mm less precipitation relative to the modern control, respectively.

Though modern vegetation distributions are not in equilibrium with the environment, pre-industrial vegetation distributions are assumed to be closer to equilibrium (Fig. 4a). Shrub Tundra dominates most of Beringia and the lake region with lingering evergreen taiga and deciduous forests in interior Siberia and Yukon. Biome distributions are similar to modern day vegetation described by Kolosova (1980) and Viereck and Little Jr (1975) indicating accurate near-modern biome distributions. The switch from evergreen taiga dominating most of interior Beringia to dominate shrub tundra can be attributed to lower preindustrial CO_2 coinciding with drier, Arctic conditions.

3.2 Paleoclimate simulations

3.2.1 MIS-1 (9 ka); Holocene thermal maximum

July temperatures in the MIS-1 simulation (12.4 °C) are ~ 2.1 °C warmer than pre-pre-industrial July temperatures (10.3 °C) with summer (JJA) temperatures being 1.6 °C warmer on average, relative to pre-industrial temperatures (Fig. 2a). Overall, there is a warming of interior Siberia of > 5 °C. July temperatures relative to pre-industrial exceed > 2 °C around most of the lake and Beringia.

Holocene PANN values in the model are analogous to pre-industrial precipitation and are statistically significant at the 95 % confidence interval. As expected, the Arctic Ocean basin is very dry, averaging about $200\,mm\,yr^{-1}$ of liquid precipitation. Wetter

conditions prevail over high topography and latitudes below the Arctic Circle. Somewhat drier conditions dominate the Siberian interior due to the enhanced continentality.

In the MIS-1 simulation, Lake El'gygytgyn is close to a transition zone with dominant shrub tundra to the east and deciduous forest to the west. Most of interior Siberia is deciduous forest with some desert in the central part (Fig. 4b).

3.2.2 MIS-5e (127 ka)

Overall warming of the Beringian interior in the MIS-5e simulation is $> 2\,°C$ relative to pre-industrial temperatures (Fig. 2b). Most of this warming can be attributed to the direct effects of the MIS-5e orbit, which produces high-intensity insolation anomalies of $> 50\,W\,m^{-2}$ (roughly 60–75 $W\,m^{-2}$) at the top of the atmosphere, relative to a modern orbit (Fig. 1b). According to ice core records, carbon dioxide (CO_2) concentrations during this period were about 287 ppm_v, contributing 0.132 $W\,m^{-2}$ more surface radiative forcing feedbacks with total GHG (CO_2, CH_4, and N_2O) contributions of $-0.0035\,W\,m^{-2}$ forcing relative to pre-industrial GHG ratios.

Comparisons with pre-industrial control simulations show differences of summer warmth (JJA) and MTWM maxima temperatures (+2.5, +4.2 °C), similar to comparisons with the modern control simulation (Fig. 2b). Summer warming over the GIS is +5 °C relative to pre-industrial and only $\sim 1\,°C$ warmer than modern simulations, significantly less than found in a recent ice core study (Dahl-Jensen et al., 2013). Mean annual precipitation ($\sim 401\,mm\,yr^{-1}$), is 37 $mm\,yr^{-1}$ less than pre-industrial levels, respectively. Overall, similar precipitation patterns are seen over the Arctic relative to MIS-5e and the pre-industrial control scenario, which reflects both the overall wet bias in our GCM and the similar continental/ice sheet boundary conditions, in both simulations.

A less moist, but warm high latitude environment produces dominant deciduous taiga and evergreen taiga biome distributions around the lake (Fig. 4c), with evergreen taiga being the most dominant in eastern Beringia and deciduous taiga being more domi-

nant around the lake region and most of western Beringia. Coastal Beringia around the Bering Strait and Arctic Ocean are dominated by scattered patches of dwarf and prostrate shrub tundra biomes. Both dwarf and shrub tundra biomes dominate coastal regions.

3.2.3 MIS-11c (409 ka)

In terms of boreal summer orbital forcing, MIS-11c is a long interglacial compared to the other interglacials in this study. We assume an ice-free Greenland in our MIS-11c simulations, with the ice sheet removed and replace with isostatically equilibrated (ice-free) land elevations. Additional experiments involving sea-ice extent will also be mentioned with the results outlined.

Summer insolation anomalies (relative to pre-industrial) during MIS-11c range from +45–55 W m^{-2} (Fig. 1c) allowing temperatures over the lake region during July (month of maximum insolation) to increase +2.2 °C relative to pre-industrial. Overall, mean annual summer temperatures over the circum-Arctic and the lake are 2 to 4 °C warmer than pre-industrial temperatures with the Siberian interior warming the most.

In MIS-11c simulations performed with (MIS11GIS) and without a GIS (MIS11NG), the effect on temperature at the Lake is shown to be negligible (~ 0.3 °C). Geopotential height anomalies at 500 hPa (+4–10 m) indicate upper-level warming east of the lake, and cooling west of the lake, but the net effect of ice sheet loss on surface air temperatures is mostly limited to Greenland itself and the proximal ocean, with little effect at the distance of Lake E, as shown in other modeling studies (Koenig et al., 2012; Otto-Bliesner et al., 2006).

The warmer MIS-11c climate and possible reductions of Greenland and West Antarctic ice sheet sheets are thought to have contributed to sea levels by as much as > 11 m (Raymo and Mitrovica, 2012) higher than today, with possibly reduced Arctic sea ice. In order to test the influence of high sea levels and an a mostly ice-free Arctic Ocean on Lake El'gygytgyn climate, heat flux convergence under sea ice was increased from 2 W m^{-2} to 10 W m^{-2} in the slab ocean/dynamic sea ice model. The resulting reductions

in sea ice extent and warmer (~ 0.2–$1.0\,°C$) (Fig. 3a) Arctic SST's produced negligible warming in the Beringian interior around the lake ($< 0.7\,°C$).

Precipitation amounts at the lake during MIS11GIS are close to modern amounts of $475\,mm\,yr^{-1}$. Also, MIS11NG exhibits the same precipitation amounts as our pre-industrial control run ($\sim 438\,mm\,yr^{-1}$). Conditions in the Arctic Ocean basin are very dry, $\sim 200\,mm\,yr^{-1}$, as expected. On the contrary, simulations of MIS11NG show reduced precipitation amounts of $-37\,mm\,yr^{-1}$ relative to MIS11GIS. Runs with increased sub-ice oceanic heat flux balanced out the loss of precipitation and produced values exactly matching rainfall rates of modern control values ($\sim 478\,mm\,yr^{-1}$).

A warmer and wetter MIS-11c places Lake El'gygytgyn on the border of evergreen taiga and shrub tundra biomes (Fig. 4d). Most of interior Siberia remains deciduous forest and temperate grassland, similar to MIS-5e and 1. Most of eastern Beringia is mostly evergreen taiga and some deciduous forest toward the northern shore of Alaska, with sporadic patches of shrub tundra mixed in. With the loss of the GIS, Greenland is now predominantly shrub tundra with dwarf shrub tundra along the northern shore. Vegetation limits, such as tree lines, are slightly changed during our simulations with increased heat flux and a warmer, open Arctic Ocean. Evergreen forests around the lake region extend poleward to the coast and slightly eastward. In western Beringia, northern coast Alaskan vegetation is shifted from predominantly evergreen forests to dwarf shrub tundra environments with a slight eastward increase of evergreen biome toward the Yukon.

3.2.4 MIS-31 (1072 ka)

An extreme warm orbit with high obliquity, high eccentricity and precession aligning perihelion with boreal summer allows insolation anomalies to be $> 50\,W\,m^{-2}$ at the surface and $+ 60$–$80\,W\,m^{-2}$ (Fig. 1d) at the top of the atmosphere at the latitude of Lake E. Average summer temperatures around the lake are about $+3.6\,°C$ warmer than pre-industrial (Fig. 2d). While MIS-31 is beyond the temporal range of ice core greenhouse gas records, proxy geochemical record imply MIS-31 has the highest $p\mathrm{CO}_2$

of the mid-Pleistocene (Hönisch et al., 2009), contributing $\sim +0.80\,\mathrm{W\,m^{-2}}$ relative to pre-industrial values. As a result, modeled July temperatures exceed $+5\,^\circ$C warmer than pre-industrial temperatures. Most summer warming is over Greenland and interior Siberia with temperatures over a presumably ice-free Greenland of $+15$–$17\,^\circ$C and in-
terior Siberia, with temperatures $+6$–$8\,^\circ$C warmer relative to pre-industrial and modern temperatures.

Overall precipitation in the Arctic during MIS-31 is $\sim 438\,\mathrm{mm\,yr^{-1}}$, similar to that of MIS-11c. Vegetation distribution is similar to the other interglacials described here (Fig. 4e). Most of the eastern Beringian (Alaska) interior is dominated by ever-
green taiga forest with only a few areas of shrub tundra along the coasts. The Lake El'gygytgyn region is dominated by deciduous taiga with evergreen dominating toward the eastern coast. Most of interior Siberia shifts from predominantly deciduous forest to only 50 % deciduous forest, with an expanding area of temperate grasslands.

3.2.5 Glacial boundary conditions

Mean Temperature of the Coldest Month (MTCM; Jan.) around Lake El'gygytgyn was simulated to be $-40\,^\circ$C with July temperatures reaching $\sim 3\,^\circ$C (Fig. 7b). These temperatures compare favorably with proxy reconstructions after 2.7 Ma (Brigham-Grette et al., 2013; Melles et al., 2012). Mean annual temperatures in the circum-Arctic decrease 5 to $25\,^\circ$C (Fig. 7c) in response to the increase of large ice sheets with respect to
the experiment run without North Hemispheric ice sheets. Most of the circum-Arctic experiences very arid conditions with more then $150\,\mathrm{mm\,yr^{-1}}$ decrease in precipitation in parts of the Arctic basin and northern Beringia (Fig. 7a). Aridification is also consistent with drying seen in Melles et al. (2012) and Brigham-Grette et al. (2013) during Pleistocene glacial periods. Aridification, while not definitive, suggests that large Northern
Hemisphere ice sheets initiation changes in the Arctic hydrologic cycle.

Title Page

Abstract   Introduction

Conclusions   References

Tables   Figures

◄◄   ►►

◄   ►

Back   Close

Full Screen / Esc

Printer-friendly Version

Interactive Discussion

4   Discussion

The exceptionally warm periods of Marine Isotope Stage(s) 1, 5e, 11c and 31 show significant, but similar changes in the Arctic, especially around Lake El'gygytgyn. Temperature reconstructions during the Holocene Thermal Maximum (9 ka) indicate +1.6 (±0.8) °C warming in the western Arctic (Kaufman and Brigham-Grette, 1993) with an overall warming of 1.7 (±0.8) °C in the circum-Arctic (Miller et al., 2010), relative to modern temperatures. Though our model does not fully account for all the warming relative to modern temperatures during this period, it does reflect the important warming in the western Arctic as documented by Kaufman and Brigham-Grette (1993). With the decrease in Arctic moisture and low CO_2, deciduous and evergreen forests dominate the Arctic landscape with tree species such as *Alnus, Betula* (nut bearing trees and fruits), *Poaceae* (grasses) and some birch and alder (Melles et al., 2012).

   Marine Isotope Stage 5e produced the greatest summer warming amongst all four interglacials modeled here. Comparisons with pre-industrial control runs show that differences in MTWM maxima at Lake El'gygytgyn during MIS-1 and 5e (+2.1 and +4.2 °C) are similar range of MIS-11c and 31 (+2.2 and +3.5 °C). Similar temperature differences have been seen in modeling studies using intermediate complexity models that also showed that a high obliquity and high eccentricity with precession aligning perihelion with boreal summer will yield the warmest boreal summer temperatures (Koenig et al., 2011; Otto-Bliesner et al., 2006; Yin and Berger, 2011). Arctic temperature reconstructions for the MIS-5e thermal maximum are variable, indicating +5 (±1) °C average warming across the entire arctic, with smaller anomalies reconstructed for the terrestrial, Pacific sector (Miller et al., 2010). Strong insolation forcing at these latitudes permits July maximum temperatures to exceed both pre-industrial and modern temperatures by > 3 °C, which is in agreement with a study done by CAPE-Last Interglacial Project Members (2006) . The 2–4 °C warming in Siberia and western Beringia in our results has also been shown by CAPE (2006), Lozhkin and Anderson (1995); Lozhkin et al. (2006) and in simulations using a GCM without vegetation feedbacks,

and has been linked to the summer insolation anomaly (Otto-Bliesner et al., 2006). Moreover, the exceptional summer warmth of MIS-5e compared to other interglacials was thought to have caused a reduction in the Greenland Ice Sheet adding 1.6 to 2.2 m of equivalent sea level rise (Colville et al., 2011). A more recent study conducted by the North Greenland Eemian Ice Drilling Project (NEEM) confirmed that the thickness of the Northwest sector of the GIS decreased by 400 ± 250 m reaching surface elevations of 130 ± 300 m lower than present (Dahl-Jensen et al., 2013). This indicates that our simulations of MIS-5e with a near-modern GIS are a good approximation for this period. Increased warmth allows almost a full replacement of shrub tundra with deciduous forest in and around the lake region. Pollen analysis during this period show tree species of birch, alder, pine and spruce (Melles et al., 2012). However, multiproxy studies of MIS-5e show a change in MTWM of only $+2\,°C$ warming at the lake compared to modern temperatures (Melles et al., 2012). It can be concluded that a warm summer orbit with only moderate GHG concentrations does account for exceptionally warm temperatures in Beringia however, the particularly muted response in the Lake El'gygytgyn proxy record to summer insolation forcing cannot be fully explained.

Simulations of MIS-11c exhibit another very warm interglacial in the Arctic around the lake with MTWM maxima approaching $+2.2\,°C$ warmer than pre-industrial temperatures. Similarly to MIS-5e and 1, peak warmth coincides with perihelion during boreal summer, however low eccentricity and obliquity attenuates the effects of precession relative to 5e and 1, making summer insolation less intense. A combination of eccentricity, obliquity and precession elevates summer insolation for ~ 45 ka, much longer than the shorter duration cycle, but a more intense summer insolation anomaly is present during MIS-5e. The overall warmth of MIS-11 is, in part, an outcome of reduced snow and ice cover. Another possible mechanism contributing to Beringian warmth at MIS-11 might be related to WAIS (Naish et al., 2009) and GIS (Koenig et al., 2011; Willerslev et al., 2007) retreat contributing to increased sea level (Raymo and Mitrovica, 2012), and increased Bering Strait throughflow. Today, the Bering straight is limited to ~ 50 m in depth with a net northward transport of ~ 0.8 Sv (Woodgate et al., 2010). Oceanic

heat transport into the Arctic basin might have been elevated during high sea level, providing a source of warm water intrusion into the Arctic Ocean basin from the North Pacific Ocean. As a simple test of the potential for a warmer Arctic Ocean with less sea ice to affect temperatures over terrestrial Beringia, heat flux convergence under sea ice in the Arctic Ocean was increased from 2 to $10\,\mathrm{W\,m^{-2}}$. Summer sea ice fraction was reduced by 25–50 % and summer ocean temperatures warmed by 0.2–1.0 °C (Fig. 3a and b). The warmer Arctic Ocean warmed the lake region, but only slightly (+0.7 °C), and does not account for the exceptional warmth of MIS-11c relative to MIS-5e.

The influence of MIS-11c temperatures on terrestrial biome distributions is supported by a poleward advance of evergreen needle-leaf forest around the lake, which is in good agreement with palynological analysis of tree species in the lake area (Melles et al., 2012) showing forest-tundra and northern larch-taiga dominated by spruce, pine, birch, alder and larch (Melles et al., 2012). Surface warming as a result of increased low albedo needle-leaf forests accounts for some of the warming during this period however, isolated forcing feedback of increased evergreen, terrestrial forest provides a net cooling effect during the summers and slight net warming effect during early fall (September–November; +0.3 °C). Evapotranspiration in the high canopies of needle-leaf forests absorb summer energy allowing the surface and canopy to cool. During cooler seasons, such as fall and winter, trees act as a blanket insulating the surface while frictional forces lessen winds near the surface.

A deglaciated Greenland has been shown to have regional effects on SSTs and sea-ice conditions, however warming of the circum-Arctic has been shown to be minimal (Koenig et al., 2012; Otto-Bliesner et al., 2006). This was demonstrated in our simulations by isolating the effects associated with the loss of the GIS leading to warming around the lake of only +0.3 °C. Analysis of 500 hPa geopotential height anomalies exhibit ridging (positive height anomalies of > 10 m) and troughing (negative height anomalies) to the west of the lake, indicating a slight change in the large-scale, synoptic planetary wave patterns over Beringia. Over the lake, positive height anomalies are also present, indicating slightly warmer conditions and a slight eastward shift of an

A. J. Coletti et al.

atmospheric ridge that may have been set up further west of the lake. The ridging in these simulations may also be related to a decrease in precipitation at the Lake when the GIS was removed. Extended high pressure over Beringia associated with ridging would create somewhat drier conditions for the region. If the exceptional warmth of MIS-11c is indeed related to the melting of the GIS, there could have been an effect on ocean overturning, resulting in a net cooling effect on the Northern Hemisphere rather than warming. Furthermore, it is not clear why the GIS would have survived MIS-5e warmth, and not MIS-11c. In sum, the exceptional Arctic warmth of MIS-11c remains difficult to explain and is not a straightforward result of greenhouse gases, orbital forcing, vegetation feedbacks, or Arctic Ocean warming.

Elevated GHG concentrations and a very warm orbit with a large precession can explain much of the warmth during MIS-31, assuming atmospheric CO_2 was higher during late Pleistocene interglacials (Hönisch et al., 2009). In the model, the combination of elevated greenhouse gases and strong summer insolation forcing at 1072 ka allow thick needle-leaf and deciduous forests to grow. Simulated summer temperatures are about 12 °C, +2 °C warmer than modern summer temperatures around the lake. Biome model simulations derived from pollen analysis inside the lake core show maxima of trees and shrubs during peak Northern Hemisphere insolation of MIS-31 at 1072 ka. Our BIOME4 model simulations also show similar results around the lake region with increased boreal forests and less tundra and small dwarf shrubs. The snow-albedo effect combined with thick low albedo, forest cover allows temperatures to increase in the Arctic during MIS-31. Peak precipitation rates derived from proxy analysis indicate about 600 mm yr^{-1}, or about 350 mm yr^{-1} more precipitation than modern model simulations (Melles et al., 2012). GCM results indicate ∼490 mm yr^{-1}, the most annual precipitation out of all four interglacials simulated here. Although modeling studies do not fully simulate the enhanced precipitation indicated in the proxy record, a relative increase in precipitation is evident in both the model and proxy records. Extraordinary warmth during MIS-31 correlates well with a diminished West Antarctic Ice Sheet (WAIS) (Pollard and DeConto, 2009) implying strong intrahemispheric coupling that has

been related to possible reductions in Antarctic Bottom Water (AABW) formation during times of ice-shelf retreat and increased fresh water input into the Southern Ocean (Foldvik, 2004). WAIS collapse could somehow be linked with the Beringian warmth during MIS-11c and MIS-5e, but definitive evidence of WAIS retreat during these late Pleistocene interglacials is currently lacking (McKay et al., 2012).

Arctic aridification and temperature change can be linked to mechanical atmospheric forcing associated with large Northern Hemisphere ice sheets. Exceptionally large temperature decreases are thought to be associated with albedo-enhanced cooling from large ice sheets reflecting solar radiation back to the atmosphere. Likewise, enhanced cooling in the Arctic and expanded sea-ice cover contributed to circum-Arctic aridification ($> 150\,\mathrm{mm\,yr^{-1}}$).

Comparable studies (Bromwich et al., 2004) using regional climate models to quantify mechanical forcing of large Northern Hemisphere ice sheets show important effects on mid-tropospheric westerly flow. The presence of a very large Laurentide ice sheets splits the jet stream into two branches: a northern most, polar jet and a southern branch (Fig. 5). During winter (January) (Fig. 5b), surface cyclones from the Arctic flow along the periphery of a mid-level high-pressure system tracking most winter storms around the southern extent of the Laurentide ice sheet. Due to a strong mid-level trough that forms on the south coast of western Beringia, storms are frequent along the southern coast of Alaska and Beringia (Bromwich et al., 2004). During the summer (July) (Fig. 5c), the jet stream is positioned directly over the ice sheet allowing increased frequency of surface cyclones to migrate directly over the ice sheet dropping 42 % of annual precipitation (Bromwich et al., 2004). This can be attributed to a large trough centered over southwest North America, allowing the storm track to push storms further south over this region and North America. Additionally, Beringia is encased in high-pressure, presumably limiting precipitation in Beringia and at the lake (Fig. 6a and b). Anomalously strong high-pressure over the lake region may be related to a strengthening of the Siberian high during periods of large glacial extent in the region. This study, along with Bromwich et al. (2004), suggest that mechanical forcing due to the presence

of large Northern Hemisphere ice sheets contributed to changes in synoptic weather patterns leading to aridification of Lake El'gygytgyn and the change of boreal/evergreen forest around the lake to shrub tundra, lichen and mosses.

5 Conclusions

Lake El'gygytgyn provides a high-resolution terrestrial proxy record of climate variability in the Arctic. A linked climate modeling study described here shows that Arctic summers were significantly warmer during several Pleistocene interglacials by as much as + 2 °C during MIS-1 and 11c, and by as much as + 4 °C during MIS-5e and 31 relative to pre-industrial. It can be inferred that the simulations experienced similar warming that was caused by a combination of elevated GHGs, and warm boreal summer orbits that lead the way for the super-interglacials in the Arctic. Although most of the interglacials have lower CO_2 than today, astronomical forcing was the dominant warming mechanism producing high-intensity summer insolation of $> 50\,W\,m^{-2}$ with respect to modern orbital configuration as seen in MIS-5e and 31. MIS-1 is an exception with lower CO_2 around the time of peak Holocene warmth producing $-0.44\,W\,m^{-2}$ less radiative forcing relative to pre-industrial levels (Melles et al., 2012). Other factors such as changes in Antarctic Bottom Water (AABW) production and reduced Arctic sea-ice may have also contributed to exceptional warmth during this time. Thorough testing of these ideas will require additional simulations with coupled atmosphere-ocean models, changes in glacial and interglacial eustatic sea-levels, changes in continentality, changes in sea-ice distributions and the addition of melt-water inputs into northern and Southern Hemisphere oceans.

Extreme interglacial warmth shifted vegetation from mostly tundra with small shrubs as we see the Arctic today to thick, lush evergreen and boreal forest. Due to the extreme warmth, wetter conditions prevailed during the super-interglacials allowing forest biomes to thrive and increase their maximum extent poleward while making each interglacial unique based upon the different tree and shrubs species that dominant during

each specific period. Ice sheets in the Arctic, such as the Greenland Ice Sheet, were significantly reduced during some interglacials, allowing summer temperatures to increase almost 2 to 5 °C warmer than present over Greenland, but with limited impact on temperatures in the lake region. The observed response of Beringia's climate and terrestrial vegetation to super-interglacial forcing is still not fully understood and creates a challenge for climate modeling and for quantifying the strength of Arctic amplification. For example, MIS-11c is the warmest observed interglacial studied here, while MIS-5e is the warmest simulated by the model. The model produces overall drier conditions in the earlier interglacials (11c and 31) relative to pollen analysis. The significant warming in the circum-Arctic can be linked to major deglaciation events in Antarctica, demonstrating possible intrahemispheric linkages between the Arctic and Antarctic climate on glacial-interglacial timescales, which have yet to be mechanistically explained.

Large Northern Hemisphere ice sheets during major glaciation events can be linked to Arctic aridification and extremely cold annual temperatures. The combination of increased Arctic sea ice and increased surface albedo allows the Arctic to significantly cool and dry out during these events. This is demonstrated in the Lake El'gygytgyn core by multiproxy analyses and a transition to shrub vegetation due to the lack of precipitation. The climate modeling showed here suggests extreme Arctic aridification after 2.7 Ma was a consequence of the episodic expansion of ice sheets, which affected dominant atmospheric pressure patterns, the storm track and a general southward shift of precipitation in the Beringian sector of the Arctic.

References

Alder, J. R., Hostetler, S. W., Pollard, D., and Schmittner, A.: Evaluation of a present-day climate simulation with a new coupled atmosphere-ocean model GENMOM, Geosci. Model Dev., 4, 69–83, doi:10.5194/gmd-4-69-2011, 2011.

Berger, A.: Long-term variations of daily insolation and quaternary climatic changes, J. Atmos. Sci., 35, 2362–2367, 1978.

A GCM comparison of Plio–Pleistocene interglacial–glacial periods

A. J. Coletti et al.

Title Page

Abstract | Introduction

Conclusions | References

Tables | Figures

◄ | ►

◄ | ►

Back | Close

Full Screen / Esc

Printer-friendly Version

Interactive Discussion

Brigham-Grette, J., Melles, M., Minyuk, P. E., Andreev, A., Tarasov, P., DeConto, R., Koenig, S., Nowaczyk, N., Wennrich, V., Rosen, P., Haltia-Hovi, E., Cook, T., Gebhardt, C., Meyer-Jacob, C., Snyder, J., and Herzschuh, U.: Pliocene warmth, polar amplification, and stepped Pleistocene cooling recorded in NE Arctic Russia, J. Science, 340, 1421–1427, 2013.

Bromwich, D. H., Toracinta, E. R., Wei, H., Oglesby, R. J., Fastook, J. L., and Hughes, T. J.: Polar MM5 simulations of the winter climate of the Laurentide Ice Sheet at the LGM*, J. Climate, 17, 3415–3433, 2004.

CAPE – Last Interglacial Project Members: Last interglacial Arctic warmth confirms polar amplification of climate change, Quaternary Sci. Rev., 25, 1383–1400, 2006.

Colville, E. J., Carlson, A. E., Beard, B. L., Hatfield, R. G., Stoner, J. S., Reyes, A. V., and Ullman, D. J.: Sr-Nd-Pb isotope evidence for ice-sheet presence on Southern Greenland during the last interglacial, Science, 333, 620–623, 2011.

Dahl-Jensen, D., and NEEM Community Members: Eemian interglacial reconstructed from a Greenland folded ice core, Nature, 493, 489–494, 2013.

De Vernal, A. and Hillaire-Marcel, C.: Natural variability of Greenland climate, vegetation, and ice volume during the past million years, Science, 320, 1622–1625, 2008.

DeConto, R. M., Galeotti, S., Pagani, M., Tracy, D., Schaefer, K., Zhang, T., Pollard, D., and Beerling, D. J.: Past extreme warming events linked to massive carbon release from thawing permafrost, Nature, 484, 87–91, 2012.

Elias, S. A. and Matthews Jr., J. V.: Arctic North American seasonal temperatures from the latest Miocene to the Early Pleistocene, based on mutual climatic range analysis of fossil beetle assemblages, Can. J. Earth Sci., 39, 911–920, 2002.

Foldvik, A.: Ice shelf water overflow and bottom water formation in the southern Weddell Sea, J. Geophys. Res., 109, 1–15, 2004.

Hönisch, B., Hemming, N. G., Archer, D., Siddall, M., and McManus, J. F.: Atmospheric carbon dioxide concentration across the Mid-Pleistocene Transition, Science, 324, 1551–1554, 2009.

Kalnay, E., Kanamitsu, M., Kistler, R., Collins, W., Deaven, D., Gandin, L., Iredell, M., Saha, S., White, G., Woollen, J., Zhu, Y., Leetmaa, A., Reynolds, R., Chelliah, M., Ebisuzaki, W., Higgins, W., Janowiak, J., Mo, K. C., Ropelewski, C., Wang, J., Jenne, R., and Joseph, D.: The NCEP/NCAR 40 year reanalysis project, B. Am. Meteorol. Soc., 77, 437–471, 1996.

Kaplan, J. O.: Climate change and Arctic ecosystems: 2. Modeling, paleodata-model comparisons, and future projections, J. Geophys. Res., 108, 1–17, 2003.

Full Screen / Esc

Printer-friendly Version

Interactive Discussion

Kaufman, D. S. and Brigham-Grette, J.: Aminostratigraphic correlations and paleotemperature implications, Pliocene–Pleistocene high-sea-level deposits, northwestern Alaska, Quaternary Sci. Rev., 12, 21–33, 1993.

Kitoh, A. and Murakami, S.: Tropical Pacific climate at the mid-Holocene and the Last Glacial Maximum simulated by a coupled ocean-atmosphere general circulation model, Paleoceanography, 17, 19-1–19-13, 2002.

Koenig, S. J., DeConto, R. M., and Pollard, D.: Late Pliocene to Pleistocene sensitivity of the Greenland Ice Sheet in response to external forcing and internal feedbacks, Clim. Dynam., 37, 1247–1268, 2011.

Koenig, S. J., DeConto, R. M., and Pollard, D.: Pliocene Model Intercomparison Project Experiment 1: implementation strategy and mid-Pliocene global climatology using GENESIS v3.0 GCM, Geosci. Model Dev., 5, 73–85, doi:10.5194/gmd-5-73-2012, 2012.

Kolosova, L.: Geographical Atlas, 1980.

Lisiecki, L. E. and Raymo, M. E.: A Pliocene–Pleistocene stack of 57 globally distributed benthic δ^{18}O records, Paleoceanography, 20, PA1003, doi:10.1029/2004PA001071, 2005.

Loulergue, L., Schilt, A., Spahni, R., Masson-Delmotte, V., Blunier, T., Lemieux, B., Barnola, J.-M., Raynaud, D., Stocker, T. F., and Chappellaz, J.: Orbital and millennial-scale features of atmospheric CH_4 over the past 800 000 years, Nature, 453, 383–386, 2008.

Lozhkin, A. V. and Anderson, P. M.: The last interglaciation in Northeast Siberia, Quaternary Res., 43, 147–158, 1995.

Lozhkin, A. V., Anderson, P. M., Matrosova, T. V., and Minyuk, P. S.: The pollen record from El'gygytgyn Lake: implications for vegetation and climate histories of northern Chukotka since the late middle Pleistocene, J. Paleolimnol., 37, 135–153, 2006.

Lüthi, D., Le Floch, M., Bereiter, B., Blunier, T., Barnola, J.-M., Siegenthaler, U., Raynaud, D., Jouzel, J., Fischer, H., Kawamura, K., and Stocker, T. F.: High-resolution carbon dioxide concentration record 650 000–800 000 years before present, Nature, 453, 379–382, 2008.

McKay, R., Naish, T., Powell, R., Barrett, P., Scherer, R., Talarico, F., Kyle, P., Monien, D., Kuhn, G., Jackolski, C., and Williams, T.: Pleistocene variability of Antarctic Ice Sheet extent in the Ross Embayment, Quaternary Sci. Rev., 34, 93–112, 2012.

Melles, M., Brigham-Grette, J., Minyuk, P. S., Nowaczyk, N. R., Wennrich, V., DeConto, R. M., Anderson, P. M., Andreev, A. A., Coletti, A., Cook, T. L., Haltia-Hovi, E., Kukkonen, M., Lozhkin, A. V., Rosen, P., Tarasov, P., Vogel, H., and Wagner, B.: 2.8 Million Years of Arctic climate change from Lake El'gygytgyn, NE Russia, Science, 337, 315–320, 2012.

A GCM comparison of Plio–Pleistocene interglacial–glacial periods

A. J. Coletti et al.

Title Page

Abstract | Introduction

Conclusions | References

Tables | Figures

◀◀ | ▶▶

◀ | ▶

Back | Close

Full Screen / Esc

Printer-friendly Version

Interactive Discussion

Miller, G. H., Alley, R. B., Brigham-Grette, J., Fitzpatrick, J. J., Polyak, L., Serreze, M. C., and White, J. W. C.: Arctic amplification: can the past constrain the future?, Quaternary Sci. Rev., 29, 1779–1790, 2010.

Naish, T., Powell, R., Levy, R., Wilson, G., Scherer, R., Talarico, F., Krissek, L., Niessen, F., Pompilio, M., Wilson, T., Carter, L., DeConto, R., Huybers, P., McKay, R., Pollard, D., Ross, J., Winter, D., Barrett, P., Browne, G., Cody, R., Cowan, E., Crampton, J., Dunbar, G., Dunbar, N., Florindo, F., Gebhardt, C., Graham, I., Hannah, M., Hansaraj, D., Harwood, D., Helling, D., Henrys, S., Hinnov, L., Kuhn, G., Kyle, P., Läufer, A., Maffioli, P., Magens, D., Mandernack, K., McIntosh, W., Millan, C., Morin, R., Ohneiser, C., Paulsen, T., Persico, D., Raine, I., Reed, J., Riesselman, C., Sagnotti, L., Schmitt, D., Sjunneskog, C., Strong, P., Taviani, M., Vogel, S., Wilch, T., and Williams, T.: Obliquity-paced Pliocene West Antarctic ice sheet oscillations, Nature, 458, 322–328, 2009.

Nolan, M. and Brigham-Grette, J.: Basic hydrology, limnology, and meteorology of modern Lake El'gygytgyn, Siberia, J. Paleolimnol., 37, 17–35, 2006.

Otto-Bliesner, B. L., Marshall, S. J., Overpeck, J. T., Miller, G. H., Hu, A., and CAPE Last Interglacial Project Members: Simulating Arctic climate warmth and icefield retreat in the last interglaciation, Science, 311, 1751–1753, 2006.

Peltier, W. R.: Ice age paleotopography, Science, 265, 195–201, 1994.

Pollard, D. and DeConto, R. M.: Modelling West Antarctic ice sheet growth and collapse through the past five million years, Nature, 458, 329–332, 2009.

Prokopenko, A. A., Bezrukova, E. V., Khursevich, G. K., Solotchina, E. P., Kuzmin, M. I., and Tarasov, P. E.: Climate in continental interior Asia during the longest interglacial of the past 500 000 years: the new MIS 11 records from Lake Baikal, SE Siberia, Climacteric, 6, 31–48, 2010.

Raymo, M. E. and Mitrovica, J. X.: Collapse of polar ice sheets during the stage 11 interglacial, Nature, 483, 453–456, 2012.

Scherer, R. P., Bohaty, S. M., Dunbar, R. B., Esper, O., Flores, J.-A., Gersonde, R., Harwood, D. M., Roberts, A. P., and Taviani, M.: Antarctic records of precession-paced insolation-driven warming during early Pleistocene Marine Isotope Stage 31, Geophys. Res. Lett., 35, 1–5, 2008.

Schilt, A., Baumgartner, M., Blunier, T., Schwander, J., Spahni, R., Fischer, H., and Stocker, T. F.: Glacial–interglacial and millennial-scale variations in the atmospheric nitrous oxide concentration during the last 800 000 years, Quaternary Sci. Rev., 29, 182–192, 2010.

Full Screen / Esc

Printer-friendly Version

Interactive Discussion

Tarasov, P. E., Nakagawa, T., Demske, D., Österle, H., Igarashi, Y., Kitagawa, J., Mokhova, L., Bazarova, V., Okuda, M., Gotanda, K., Miyoshi, N., Fujiki, T., Takemura, K., Yonenobu, H., and Fleck, A.: Progress in the reconstruction of quaternary climate dynamics in the North-west Pacific: a new modern analogue reference dataset and its application to the 430 ka pollen record from Lake Biwa, Earth-Sci. Rev., 108, 64–79, 2011.

Thompson, S. L. and Pollard, D.: Greenland and Antarctic mass balances for present and doubled atmospheric CO_2 from the GENESIS version-2 global climate model, J. Climate, 10, 871–900, 1997.

Viereck, L. A. and Little Jr., E. L.: Atlas of United States Trees, vol. 2: Alaska Trees and Common Shrubs, 1975.

Willerslev, E., Cappellini, E., Boomsma, W., Nielsen, R., Hebsgaard, M. B., Brand, T. B., Hofreiter, M., Bunce, M., Poinar, H. N., Dahl-Jensen, D., Johnsen, S., Steffensen, J. P., Bennike, O., Schwenninger, J.-L., Nathan, R., Armitage, S., de Hoog, C.-J., Alfimov, V., Christl, M., Beer, J., Muscheler, R., Barker, J., Sharp, M., Penkman, K. E. H., Haile, J., Taberlet, P., Gilbert, M. T. P., Casoli, A., Campani, E., and Collins, M. J.: Ancient biomolecules from deep ice cores reveal a forested southern greenland, Science, 317, 111–114, 2007.

Woodgate, R. A., Weingartner, T., and Lindsay, R.: The 2007 Bering Strait oceanic heat flux and anomalous Arctic sea-ice retreat, Geophys. Res. Lett., 37, 1–5, 2010.

Yin, Q. Z. and Berger, A.: Individual contribution of insolation and CO_2 to the interglacial climates of the past 800 000 years, Clim. Dynam., 38, 709–724, 2011.

Title Page

Abstract | Introduction

Conclusions | References

Tables | Figures

◄ | ►

◄ | ►

Back | Close

Full Screen / Esc

Printer-friendly Version

Interactive Discussion

Table 1. Overview of interglacial simulations performed during this study. Orbital configurations (Berger, 1978) and greenhouse gas (GHG) concentrations (Honisch et al., 2009; Loulergue et al., 2008; Lüthi et al., 2008; Schilt et al., 2010). Modern GHG concentrations are taken from 1950 AD; obliquity is given in degrees and precession is Ω. Temperatures are mean July temperatures (Table from Melles et al., 2012, Supplement).

Run Name	CO_2 (ppm)	CH_4 (ppbv)	N_2O (ppbv)	Eccentricity	Obliquity	Precession	Temp (°C)	Prec. (mm yr^{-1})
pre-industrial	280	801	289	0.016706	23.438	102.94	10.3	438
modern	355	1748	311	0.016706	23.438	102.94	12.0	475
MIS 1-with GIS	∼ 260	∼ 611	∼ 263	0.019200	24.29	311.26	12.4	438
MIS 5e-with GIS	287	724	262	0.039378	24.04	275.42	14.5	401
MIS 11c-with GIS	285	713	285	0.019322	23.781	276.67	12.2	475
MIS 31-with GIS	325	800	288	0.055970	23.898	289.79	13.8	438
MIS 11c-no GIS	285	713	284	0.019322	23.781	276.67	12.5	438
MIS 11c-no GIS-10 W m^{-2}	285	713	284	0.019322	23.781	276.67	13.2	475

Table 2. List of glacial simulations. Run 3NG116K is the simulation without Northern Hemispheric ice sheets and 3HL116K has all major Northern Hemispheric ice sheets. Obliquity and Precession are in degrees (°) and GHG concentrations are labeled.

Run Name	CO_2 (ppm)	CH_4 (ppbv)	N_2O (ppbv)	Eccentricity	Obliquity	Precession
3NG116K	300	800	288	0.043988	22.52	92.71
3HL116K	300	800	288	0.043988	22.52	92.71

Full Screen / Esc

Printer-friendly Version

Interactive Discussion
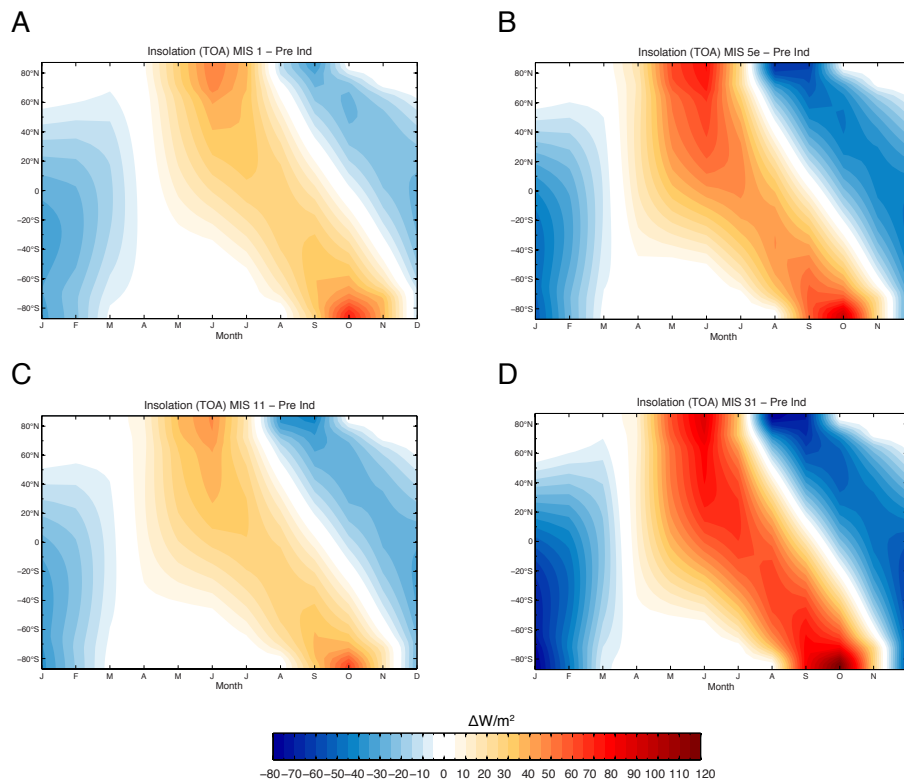
Figure 1. Monthly insolation anomalies at the top of the atmosphere for the interglacial intervals modeled here [$W\,m^{-2}$]. **(A)** MIS-1 anomalies with respect to present orbit, **(B)** MIS-5e anomalies with respect to present orbit, **(C)** MIS-11c anomalies with respect to modern orbit and **(D)** MIS-31 anomalies with respect to modern orbit.
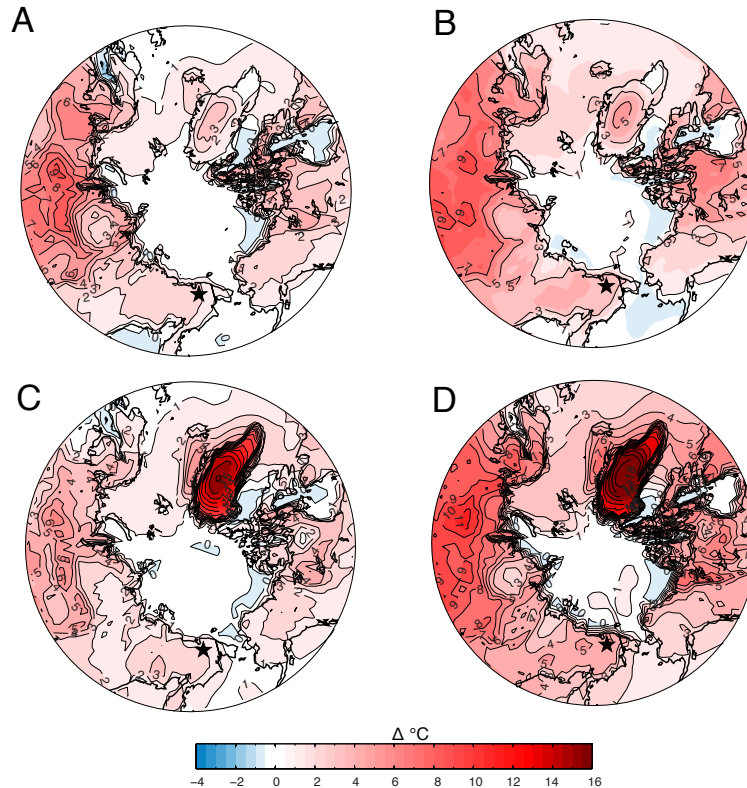
Figure 2. Simulated interglacial warming (2 m surface temperature in °C) relative to pre-industrial temperatures. **(A)** MIS-1 (9 ka orbit and GHGs), **(B)** MIS-5e (127 ka orbit and GHGs), **(C)** MIS-11c (409 ka orbit and GHGs, and no Greenland Ice Sheet), **(D)** MIS-31 (1072 ka orbit and GHGs, and no Greenland Ice Sheet). The location of Lake El'gygytgyn (black star) is shown near the bottom of each panel. Areas of no shading (white) roughly correspond to statistically significant anomalies at the 95 % confidence interval.

Title Page

Abstract | Introduction

Conclusions | References

Tables | Figures

|◀ | ▶|

◀ | ▶

Back | Close

Full Screen / Esc

Printer-friendly Version

Interactive Discussion
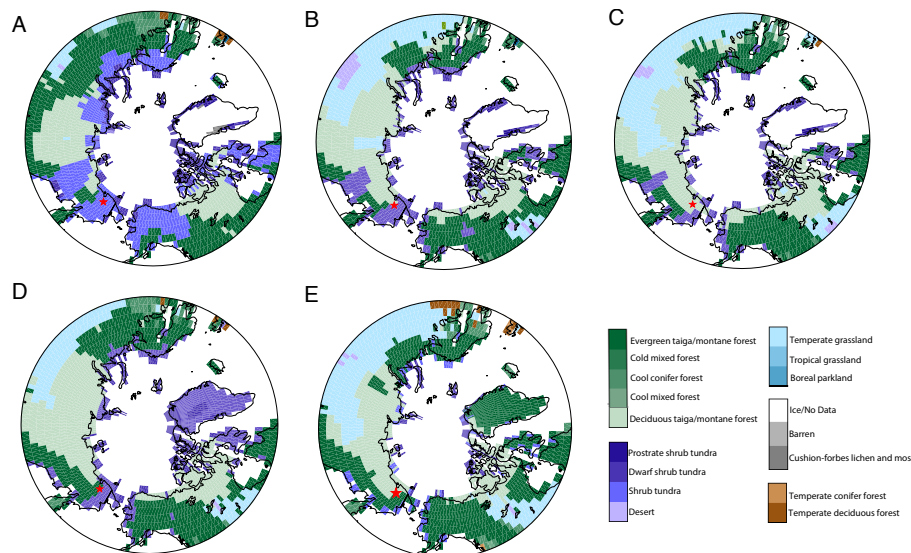
Figure 3. Distribution of interglacial vegetation simulated by the BIOME4 interactive vegetation model coupled to the GCM. **(A)** Modern vegetation corresponding to modern summer anomalies, **(B)** MIS-1 (9 ka), **(C)** MIS-5e vegetation, **(D)** MIS-11c vegetation and **(E)** MIS-31 vegetation. The location of Lake El'gygytgyn is shown near the bottom of each figure with a red star. Note the poleward advancement of evergreen and needle-leaf trees around the lake during each interglacial and the replacement of shrub tundra to taiga forest as seen in Melles et al. (2012).

Title Page

Abstract | Introduction

Conclusions | References

Tables | Figures

◀ | ▶

◀ | ▶

Back | Close

Full Screen / Esc

Printer-friendly Version

Interactive Discussion

Summer (JJA) sea surface temperature anomalies (Enhanced heat flux - Default heat flux)   Δ T °C

A

Fractional Summer (JJA) sea ice anomalies (Enhanced heat flux - Default heat flux)   Δ %

B
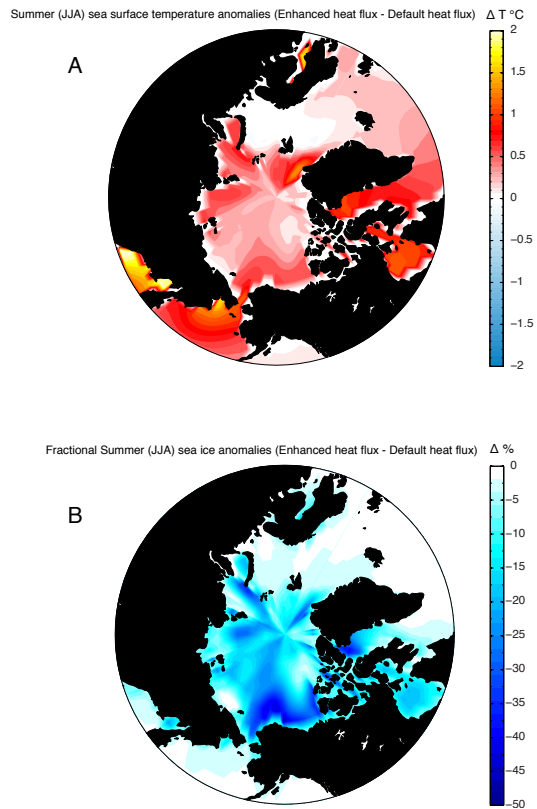
Figure 4. Summer sea surface temperature and sea ice anomalies caused by enhanced oceanic heat flux (+8 W m^{-2}). **(A)** Summer (JJA) sea surface temperature change with respect to default heat flux simulation (T °C) and **(B)** Summer (JJA) sea ice fraction anomalies (%) with respect to default heat flux simulation. With +8 W m^{-2} of sub-sea ice heat flux convergence, Arctic Ocean SSTs rise > 0.5 °C and sea ice fraction decreases 25–50 % in most areas.

Full Screen / Esc

Printer-friendly Version

Interactive Discussion
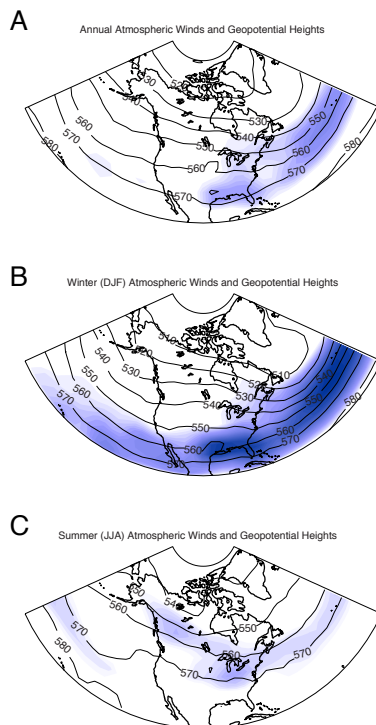
Figure 5. Seasonal distribution of 500 hPa wind [m s^{-1}] and geopotential heights over North America and the high latitudes with a Laurentide Ice Sheet. **(A)** Average annual position of jet stream, **(B)** Mean winter position of the jet stream and **(C)** Mean summer position of the jet stream. Split flow is more evident in annual and summer means. and correlate well with a Polar MM5 regional climate model study (Bromwich et al., 2004). Shaded areas are wind speeds from 15 (lightest shading) to 40 (darkest shading) in m s^{-1}.
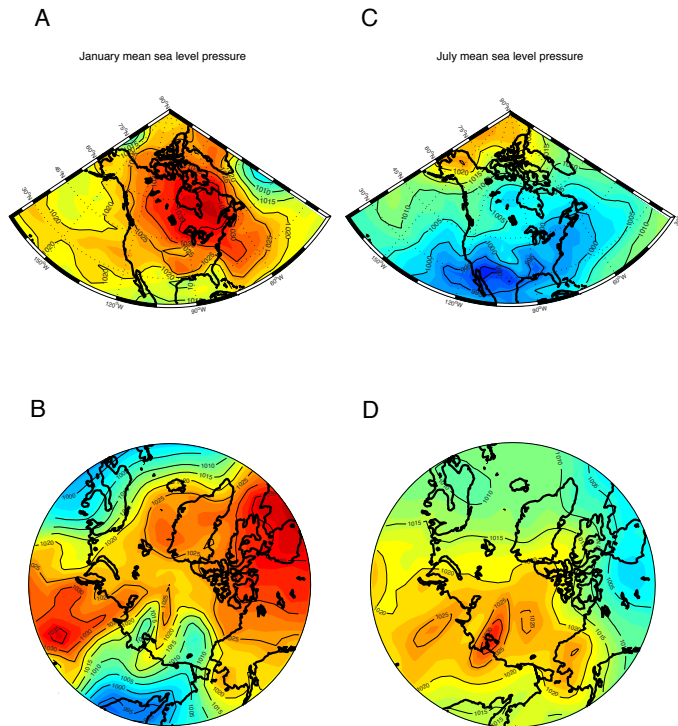
Figure 6. Climate model simulations of mean sea level pressure during January and July. Both simulations have full LGM Northern Hemisphere ice sheets. **(A)** January mean sea level pressure (MSLP) over the continental United States (CONUS), **(B)** MSLP over the Arctic Basin, **(C)** July MSLP over CONUS and **(D)** July MSLP over the Arctic Basin. Warm colors represent high MSLP and cool colors low MSLP. Note the strong high pressure over North America associated with the Laurentide ice sheet also seen in jet stream patterns during the winter (Fig. 5b). During summer, low pressure forms over North America. This is also evident in jet stream patterns (Fig. 5c).

Title Page

Abstract | Introduction

Conclusions | References

Tables | Figures

◄ | ►

◄ | ►

Back | Close

Full Screen / Esc

Printer-friendly Version

Interactive Discussion

A GCM comparison of Plio–Pleistocene interglacial–glacial periods

A. J. Coletti et al.
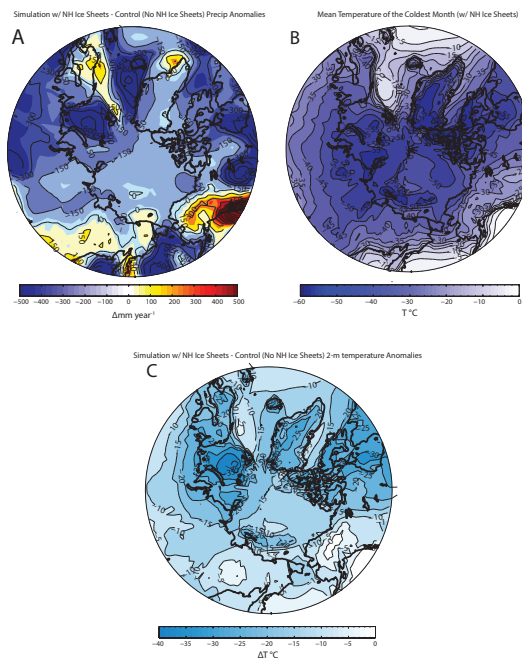
Figure 7. Climate model simulations using 300 ppm$_v$ CO_2 and a cold boreal summer orbit similar to that at 116 ka. Note the effect of large Northern Hemisphere ice sheets on the circum-Arctic with respect to aridification and cooling. **(A)** Annual precipitation anomalies (difference) of glacial conditions with respect to the same run without NH ice sheets (mm yr^{-1}), **(B)** Circum-Arctic mean temperatures of the coldest month (MTCM = January) during typical glacial conditions (°C) and **(C)** 2 m temperature anomalies (°C) with NH ice sheets, with respect to the simulations without NH ice sheets. MTCM temperatures compare favorablly with Lake El'gygytgyn proxy reconstructions after ∼ 2.9 Ma. Precipitation values are statistically significant at the 95 % confidence interval.